Submitted to J. Phys. Chem. B

Mapping the Long-Range Electron Transfer Route in Ligninolytic Peroxidases

Sandra Acebes,[†1] Francisco J. Ruiz-Dueñas,[‡] Mario Toubes,[‡2] Veronica Sáez-Jiménez,[‡3] Marta Pérez-Boada,[‡] M. Fátima Lucas,[†¶] Angel T. Martínez,*[‡] and Victor Guallar*[†§]

[†]Barcelona Supercomputing Center, Joint BSC-CRG-IRB Research Program in Computational Biology, Jordi Girona 29, E-08034 Barcelona, Spain

[‡]Centro de Investigaciones Biológicas, CSIC, Ramiro de Maeztu 9, E-28040 Madrid, Spain

[¶]Anaxomics Biotech, Balmes 89, 08008 Barcelona, Spain

[§]ICREA, Passeig Lluís Companys 23, E-08010 Barcelona, Spain

Abstract: Combining a computational analysis with site-directed mutagenesis, we have studied the long-range electron transfer pathway in versatile and lignin peroxidases, two enzymes of biotechnological interest that play a key role for fungal degradation of lignin in plant biomass. The *in silico* study established two possible electron transfer routes starting at the surface tryptophan residue previously identified as responsible for oxidation of the bulky lignin polymer. Moreover, in both enzymes, a second buried tryptophan residue appears as a top electron transfer carrier, indicating the prevalence of one pathway. Site-directed mutagenesis of versatile peroxidase (from *Pleurotus eryngii*) allowed us to corroborate the computational analysis and the role played by the buried tryptophan (Trp244) and a neighbor phenylalanine residue (Phe198), together with the surface tryptophan, in the electron transfer. These three aromatic residues are highly conserved in all the sequences analyzed (up to a total of 169). The importance of the surface (Trp171) and buried (Trp251) tryptophan residues in lignin peroxidase has been also confirmed by directed mutagenesis of the *Phanerochaete chrysosporium* enzyme. Overall, the combined procedure identifies analogous electron transfer pathways in the long-range oxidation mechanism for both ligninolytic peroxidases, constituting a good example of how computational analysis avoids making extensive trial-error mutagenic experiments.

INTRODUCTION

Ligninolytic peroxidases are heme peroxidases in class-II of the peroxidase-catalase superfamily.[1] They play a key role in lignin degradation enabling the fungal decay of wood and other lignocellulosic biomass for carbon recycling in land ecosystems.[2,3] Enzymatic delignification and lignin modification are of high biotechnological interest, having multiple potential applications from paper pulp manufacturing to the production of biofuels, chemicals and added value products in lignocellulose biorefineries, where all biomass constituents should be used.[4-6] In particular, the use of these enzymes in the above industrial processes would result in saving resources, time and money, together with reduced environmental impacts. For this reason, unveiling the molecular mechanism of the enzymatic degradation of lignin has recently centered major attention.[7-9]

All fungal ligninolytic peroxidases share a similar topology and folding, including 4-5 disulfide bridges and binding sites for two structural Ca^{2+} ions that contribute to the stability of the protein structure.[10-11] They contain an internal heme with an electron deficient iron (in its active form), responsible for the enzyme's catalytic activity. This internal prosthetic group is connected to the solvent by two channels: i) the main channel, which is conserved in all heme peroxidases and allows the entrance of hydrogen peroxide (necessary for the enzyme activation) and different small substrates; and ii) a narrow channel, specific of some of these peroxidases, located directly on the internal heme propionate (the most distant from the main channel), which has been shown to bind manganese.[12,13]

There are three families of ligninolytic peroxidases - lignin peroxidase (LiP), manganese peroxidase (MnP) and versatile peroxidase (VP) - that differ basically in the substrates that are able to oxidize at different catalytic sites.[13] MnPs are characterized by presenting a Mn-binding site at the propionate channel formed by three acidic residues (two in atypical MnPs)[14] where this cation is oxidized (Mn^{3+} acting as a diffusible oxidizer). Recently, it has been demonstrated that low redox-potential aromatic substrates can be oxidized at this catalytic site by short MnPs.[15] An equivalent Mn-

oxidation site is present in VPs, which are also able to oxidize different low redox-potential substrates at the main heme channel.[16] In addition, VPs share with LiPs the ability to oxidize high redox-potential aromatic compounds through a protein radical exposed to the solvent, which was first detected in VP[17] and later in LiP,[18] and whose direct involvement in lignin degradation has been recently shown.[19]

The catalytic cycle is similar to all ligninolytic peroxidases, involving first the (two electron) activation by hydrogen peroxide forming the (metal) electron deficient active species, compound I, which is the responsible for the first (one-electron) substrate oxidation, passing to compound II that oxidizes a second substrate molecule.[11,20] Compound I contains two unpaired electrons in an iron-oxo moiety and a third unpaired electron in a porphyrin cation radical, which is capable of oxidizing several substrates in the vicinity of the heme. However, for oxidation of lignin, or other bulky recalcitrant molecules, this radical must be transferred to a superficial residue, typically a tryptophan, through a long-range electron transfer (LRET) mechanism. Such catalytic residues have been well characterized by site-directed mutagenesis, corresponding to Trp164[19,21] in VP (isoenzyme VPL) from *Pleurotus eryngii*, and its homologous Trp171[22-25] in LiP (isoenzyme H8) from *Phanerochaete chrysosporium.*

In this work, we combine a computational analysis with site-directed mutagenesis to map the LRET pathway, tracing the residues that connect donor and acceptor in VP, and localized a similar pathway in LiP. A rigorous computational study of LRET would involve an *ab initio* quantum chemistry treatment of the system plus electronic coupling calculations. Such treatment is computationally prohibitive. However, simpler alternatives have been employed to qualitatively predict tunneling paths. For example, the module PATHWAYS, from the software HARLEM,[26] identifies the residues with higher probability to act as electron carriers using a geometrical analysis and empirical tunneling factors. In this study, we use an intermediate approach based on a mixed quantum mechanics and molecular mechanics (QM/MM) method, the QM/MM e-pathway,[27,28]

providing a semi-quantitative ranking of the residues' electron affinity. This approach has been recently used to identify the LRET route from an exposed tryptophan in a dye-decolorizing peroxidase, a member of a different superfamily also oxidizing lignin-derived products.[29] The computational study indicates two predominant paths, common in both systems, but with a clear preference for a LRET pathway involving a second (buried) tryptophan residue. Site-directed mutagenesis allowed to further corroborate the computational analysis, obtaining a detailed molecular mechanism for this important step in the enzymatic activity of ligninolytic peroxidases.

METHODS

System setup. Enzymes were prepared from the crystallographic structures (PDB entries 3FJW and 1LGA for *P. eryngii* VP and *P. chrysosporium* LiP, respectively) using the protein preparation wizard from the Schrödinger suite of programs.[30] Protonation states were adjusted with PROPKA[31] considering pH 3.0: the optimum for oxidation of the typical LiP/VP substrate veratryl alcohol (VA). In particular, the following VP residues were modified: neutral glutamic acid for residues 36, 37, 40, 83, 140, 217 and 225; neutral Asp231; protonated histidine for residues 95, 136 and 293; and neutral ε-protonated histidine for residues 39 and 232. Similarly, several amino acids were also modified in LiP: neutral glutamic acid for residues 168, 224 and 232; neutral Asp183; protonated histidine for residues 30, 82, 101, 149, 310 and 341; neutral ε-protonated His239. Partial atomic charges for the heme and VA were obtained with QM/MM simulations at the B3LYP(LACVP*)/OPLS2005 level of theory using Qsite.[32]

Substrate diffusion with PELE. Ligand diffusion and docking simulations were performed with PELE (Protein Energy Landscape Exploration),[33] a Monte Carlo based algorithm capable of accurately modeling ligand migration and its induced fit with modest computational cost. The sampling algorithm is basically composed by an initial perturbation of both receptor and the ligand, followed by the relaxation of the overall system by means of side chain sampling and minimization

steps. The resulting movement is accepted if complies the Metropolis criteria. Two different simulations were performed: i) a global one, where the substrate (VA) is free to explore the entire enzyme surface; and ii) a local one, where the ligand center of mass was constrained within a 15 Å sphere from the catalytic tryptophan α-carbon. A similar procedure has been used when studying the enzyme-substrate binding process in other peroxidases.[34]

QM/MM e-pathway calculations. LRET was characterized by the QM/MM e-pathway method,[27] a technique that ranks a set of specified residues by its tendency to host the radical during the electron transfer process (**Figure 1**).

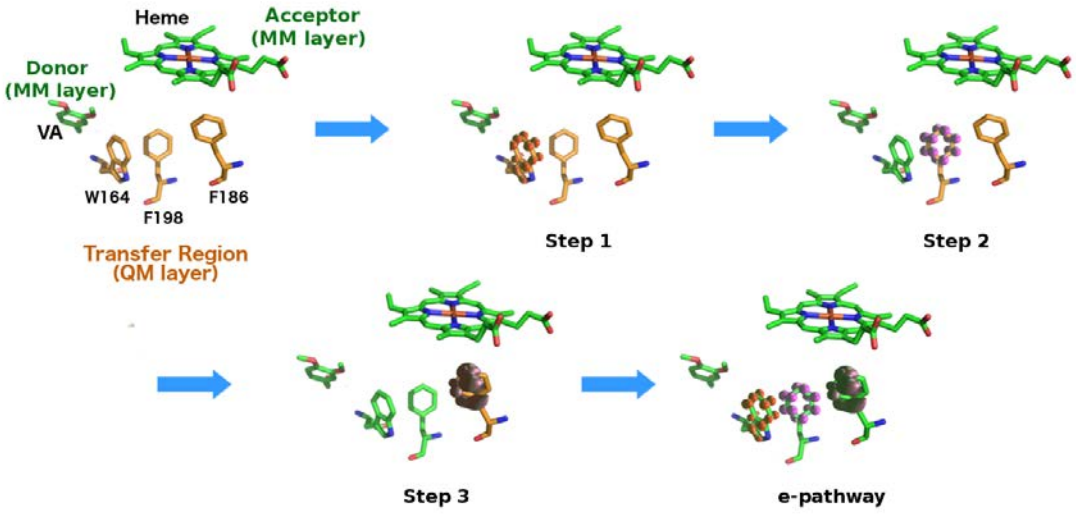

Figure 1. Illustration of QM/MM e-pathway procedure (that does not presume to represent any result).[27] The strategy consists of identifying the residue that hosts the spin density in a QM/MM calculation (step 1), where only the residues potentially involved in the transfer are placed in the QM region (in orange) whereas donor and acceptor are frozen in the MM region (in green). This residue is then subtracted from the QM region in the following calculations (steps 2 and 3) and the process is iterated until localizing a complete e-pathway (connecting donor and acceptor).

For the calculations, structures obtained after substrate diffusion with PELE were placed in an orthorhombic box of water, and the solvent was equilibrated (keeping the VA substrate and all the

protein alpha carbons frozen) with 0.5 ns of molecular dynamics simulation performed with Desmond.[35] The default relaxation protocol in Desmond was used followed by production runs using the NPT ensemble with a Nosé-Hoover thermostat and a Martyna-Tobias-Klein barostat. Then, the donor (VA) and acceptor (heme) were optimized at M06(LACVP*)/OPLS2005 level. The transfer region (keeping the previously optimized donor and acceptor groups frozen) for the QM/MM e-pathway method was then relaxed (five geometry optimization steps) at B3LYP(6-31g*)/OPLS2005 level to reduce possible structural strain.

The transfer region for QM/MM calculations in VP contains the twenty-three residues shown in **Figure 2 (left**), and homologous residues were included in the LiP calculation (**Figure 2, right**). After optimization, the iterative single point calculations of the QM/MM e-pathway method were performed at the HF(6-31g*) level of theory, since density functional theory methods tend to delocalize in excess the spin density,[36] and the residues that host the spin in each stage were ranked.

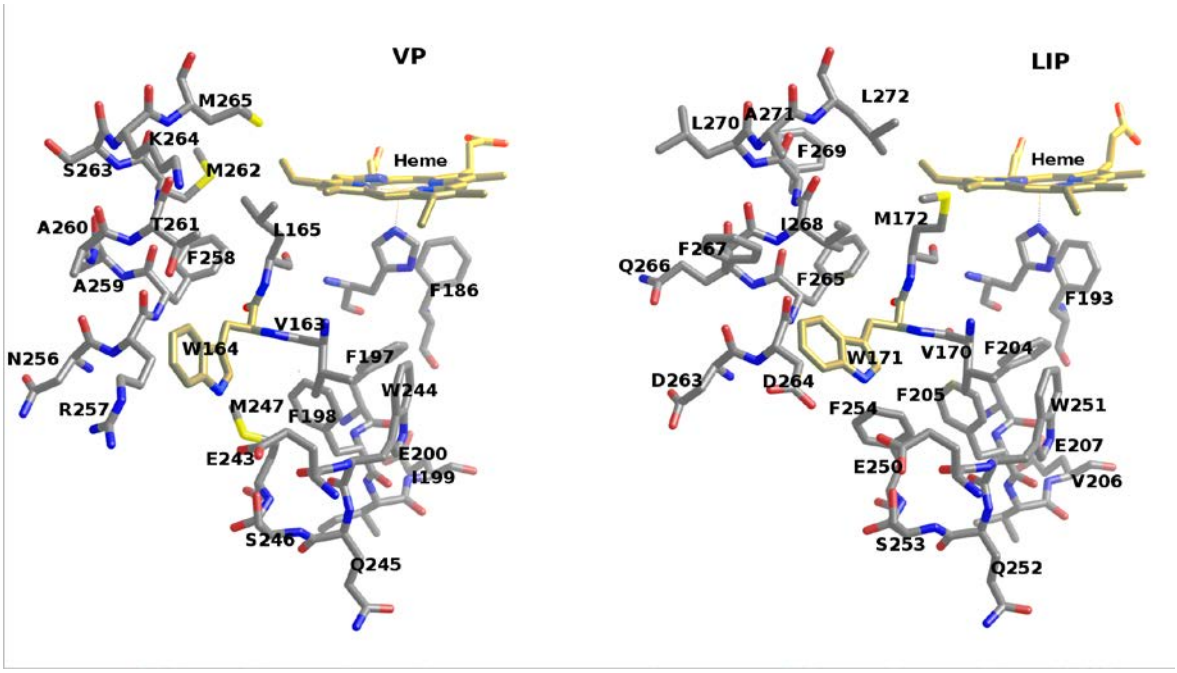

Figure 2. Residues included in the transfer region in VP (*left*) and LiP (*right*) for the QM/MM e-pathway. Recall that the proximal histidine and the heme are displayed only as a reference and they were not included in the QM transfer region. For better visualization, the enzyme cofactor (heme) and catalytic tryptophan (Trp164/Trp171) are displayed in gold.

Directed mutagenesis. Several site-directed mutations were introduced by mutagenic polymerase chain reaction (PCR) using the expression plasmid pFLAG1 (International Biotechnologies) containing the coding DNA sequence of *P. eryngii* VP (allelic variant VPL2; GenBank® accession number AF007222), named pFLAG1-VPL2, as template. For each mutation, both a direct and a reverse primers were designed complementary to opposite strands of the same DNA region containing the desired mutation. PCRs were performed (50 μL final volume) using 10 ng of template DNA, each dNTP at 500 μM, 125 ng of direct and reverse primers, 2.5 units of Pfu Turbo polymerase (Stratagene), and the manufacturers buffer. Reaction conditions were as follows: i) a *hot start* at 95ºC for 1 min; ii) 18 cycles at 95 °C for 50 s, 55°C for 50 s, and 68°C for 10 min; and iii) a final cycle at 68° C for 10 min. pFLAG1-VPL2 plasmids containing the mutations were treated with endonuclease *Dpn*I to digests methylated parental non-mutated double-stranded DNA, and transformed into *Escherichia coli* DH5α for propagation (and into *E. coli* W3110 for expression). One positive clone of each variant was selected, sequenced (PerkinElmer ABI Prism 377) and checked to confirm that the desired mutations had been properly introduced. The same procedure was followed for directed mutagenesis (W251A) of *P. chrysosporium* LiPH8 (GenBank accession number Y00262).

Heterologous expression. Wild-type recombinant VP and its directed variants were expressed in *E. coli* W3110.[37] Cells were grown in Terrific broth[38] at 37ºC until reaching an OD_{500} of ~1 (~3 h). Then protein expression was induced with 1 mM isopropyl β-D-1-thiogalactopyranoside, and cells were grown for a further 4 h. The apoenzyme was produced as inclusion bodies and then recovered in a 50 mM Tris/HCl (pH 8.0) solution containing 8 M urea, 1 mM ethylenediaminetetraacetic acid and 1 mM dithiothreitol (DTT). The subsequent *in vitro* folding of the solubilized apoenzyme was carried out in a solution of 0.16 M urea, 20 μM haemin, 5 mM $CaCl_2$, 0.1 mM DTT, 0.5 mM oxidized glutathione and 0.1 mg/ml protein, in 20 mM Tris/HCl buffer (pH 9.5) at room temperature (overnight).

The refolded enzyme was purified by Resource-Q chromatography using a 0–0.3 M NaCl gradient (2 ml/min for 20 min) in 10 mM sodium tartrate (pH 5.5) containing 1 mM $CaCl_2$. Finally, the purified enzyme was dialyzed against 10 mM sodium tartrate (pH 5). The proteins showed Reinheitszahl values (R_z, OD_{407}/OD_{280}) of ~4 confirming their high purity. Their UV–visible spectra in the 300–700 nm range confirmed that they were correctly folded.

A similar procedure was used for *E. coli* expression, *in vitro* activation and purification of the *P. chrysosporium* LiPH8 variant, using previously described conditions.[44]

Enzyme kinetics. Oxidation of VA (veratraldehyde ε_{310} 9300 $mM^{-1}\cdot cm^{-1}$) and Mn^{2+} (Mn^{3+} tartrate complex ε_{238} 6500 $M^{-1}\cdot cm^{1}$) were measured at pH 3 and pH 5, respectively. Reactions were performed in 0.1 M tartrate buffer, at 25ºC, in the presence of 0.1 mM H_2O_2. Enzymatic activities were measured as initial velocities taking linear increments of absorbance due to the appearance of the reaction product using a Shimadzu UV-1800 spectrophotometer.

Steady-state kinetic constants were calculated from the oxidation of increasing substrate concentrations until enzyme saturation was observed. Values and standard errors for apparent affinity constant (Michaelis constant, K_m) and maximal enzyme turnover (catalytic constant, k_{cat}) were obtained by nonlinear least-squares fitting to the Michaelis–Menten model. Fitting of these constants to a normalized Michaelis–Menten equation defined as $v = (k_{cat}/K_m)[S]/(1+[S]/K_m)$, where v is the reaction rate and S is the substrate concentration, yielded enzyme efficiency values (k_{cat}/K_m) with their corresponding standard errors.

RESULTS and DISCUSSION

A combination of computational and experimental efforts was performed to shed light on the LRET pathway involved in oxidation of VA (as a simple lignin model compound) by ligninolytic peroxidases.

Computational analysis of intramolecular LRET in VP. The enzymatic process was modeled at a molecular and an electronic level of detail (mapping, respectively, the protein-ligand recognition and the electron transfer) in order to identify the key amino acids involved in the LRET mechanism.

Aiming at studying the VP-VA recognition event, the ligand was placed in the bulk solvent and allowed to explore the entire protein surface. A similar complete analysis of the biophysical and biochemical events allowed us, for example, to recently engineer a highly stable MnP and activate it for oxidation of a new substrate.[34] In the present case, however, no significant minima were detected in the vicinity of Trp164, which is in agreement with the (very) low affinity observed for VA (VP K_m 4130 ± 320 μM). Analogous results were obtained when using alternative cavity detection techniques such as Sitemap, where no significant minima are detected.

Thus, following the experimental evidence that identified the superficial Trp164 as the catalytic residue[21] (whose alpha carbon is placed at 13.3 Å from the Fe metal center), VA was constrained to explore only a region within 15 Å from the tryptophan. This procedure enhances the sampling in a defined region, allowing to identify shallow local minima. As displayed in **Figure 3 (left)**, the diffusion simulation shows now a small minimum involving two hydrogen bonds between the alcohol group in VA and the HE1 hydrogen from Trp164 and the OE1 oxygen atom from Glu243, along with the stacking of Arg257 to the aromatic ring.

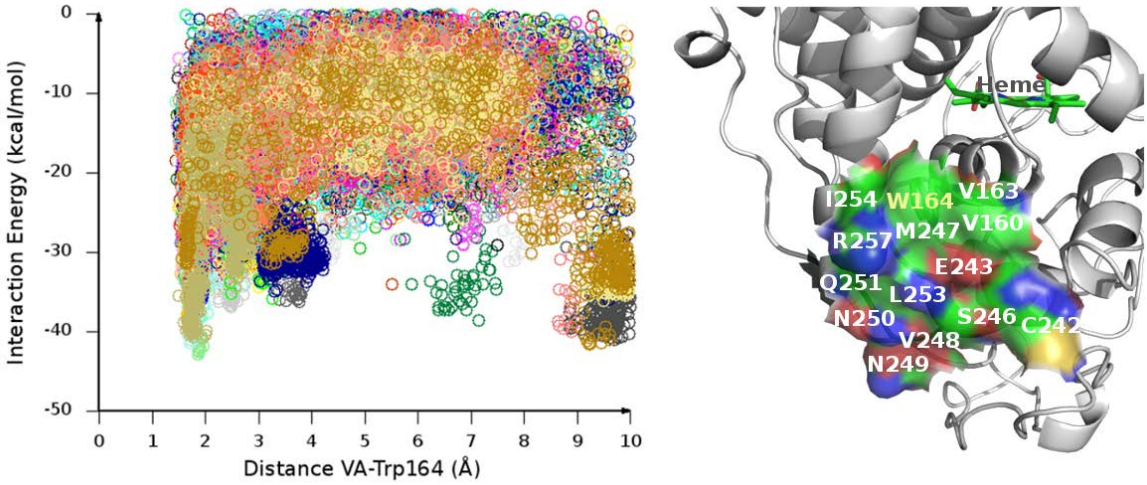

Figure 3. Substrate exploration in the environment of the catalytic Trp164 in VP. *Left*: Interaction energy (kcal/mol) *vs* the shortest (pairwise) distance from any VA atom to Trp164 (HE1 atom) in the local PELE diffusion simulations (120 cpus x 48 h, each color represents a different processor). *Right*: Set of contact residues (within 4 Å) to VA in the best interaction energy structures (within 5 kcal/mol from the local minimum).

We should emphasize, however, that VA presents several different arrangements within this local minimum. **Figure 3** shows the superficial contact residues in the different conformations found within 5 kcal/mol of the energy minimum at 2 Å. Overall, our sampling results are in agreement with a recent study combining docking and molecular dynamics techniques, where VA was found to adopt multiple orientations and a short bound life span.[39]

Five representative structures were then analyzed using the QM/MM e-pathway method, identifying for each pose the top seven residues with larger electron affinity in the transfer region. The list of residues for each set, ranked in electron affinity, and the nature of the spin density (in backbone or/and side chain) are shown in **Table 1**.

Table 1. QM/MM e-pathway results (after seven iterations) from five different snapshots (sets 1-5) taken from the local PELE diffusion of VA in VP. Residues hosting the spin are listed (from left to right) in order of electron affinity.

	QM/MM e-pathway iterations						
	1	*2*	*3*	*4*	*5*	*6*	*7*
set 1	W244	W164	F258	M265	F198 I199 (bb)[a]	M262	R257 (bb) N256 (bb)
set 2	W244 F198 (sc+bb)	W164	M265	F258	M262	R257	M247
set 3	M262 F258	W244	W164 M247	M265	F198 (bb)	F186 (bb)	R257 (bb+sc) N256 (bb)
set 4	M265	W244	F198	W164 M262	R257 (bb)	M247	F186 (bb+sc)
set 5	W164	W244	M265	M262	F258 (bb) A259 (bb)	F198 (bb) I199 (bb)	R257 (bb+sc) N256 (bb)

[a] *bb* or *bb+sc* are specified when the spin density is located only at the residue's backbone or at both backbone and side-chain, respectively (in all the other cases it is located only at the side chain).

Figure 4 locates the main residues within the VP structure and summarizes the ranking with their corresponding frequencies (qualitatively indicating their electron affinity ranking). Interestingly, there is one buried tryptophan, Trp244, that appears in all the studied sets as the top or the second residue with larger electron affinity, sometimes even before the surface catalytic residue, Trp164, suggesting a central role in the LRET. The surface Trp164 also appears in all runs: in first, second (twice), third and fourth positions. Moreover, there are two methionines, Met262 and Met265, that frequently appear in the calculation, as well as Phe198, Phe258 and Arg257. A third methionine, Met247, was not selected because it only appears in three of the computed paths (**Table 1**). The overall inspection of these residues suggests two possible electron transfer paths beginning from Trp164 (**Figure 4**): one involving Met262 and Met265, which could also comprise Arg257 and Phe258 (that we called the *Met's path*), and the other route (named the *Phe's path* and the preferred option based on the rankings) involving Trp244 and Phe198, the latter residue in the vicinity to the proximal histidine.

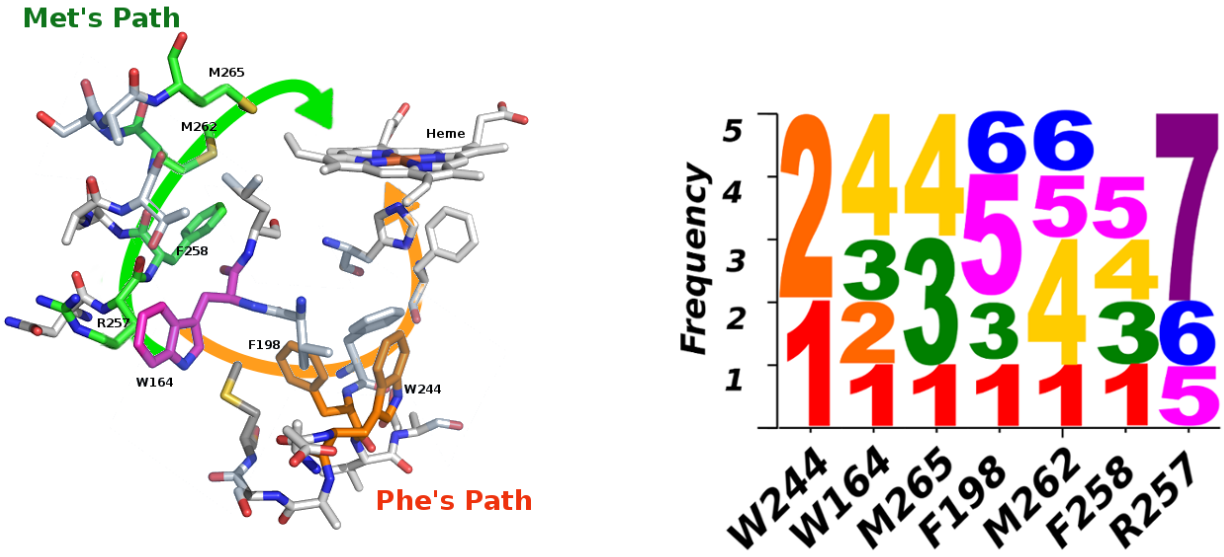

Figure 4. VP electron transfer from Trp164 to heme. *Left*: Suggested LRET routes and neighbor residues. The catalytic surface residue is displayed in pink color, whereas the main residues found in the QM/MM e-pathway are displayed in green (*Met's path*) and orange (*Phe's path*). *Right*: Frequency of the positions found in the QM/MM e-pathways (data from Table 1) for the most common residues (found, at least, in four paths).

Directed mutagenesis of VP. In order to shed light on the most probable route and verify the influence over the catalysis of the residues found in the QM/MM e-pathway, two new mutants (F198I and W244L) were obtained and experimentally characterized together with five more previously obtained (W164S, M247F, M247L, R257L and M265L). Due to the nature of the spin density for these residues, involving mainly their side chains (**Table 1**), we mutated them for leucines/isoleucines, as hydrophobic residues with a very low prospective of acting as electron carriers through its side chain (**Table 2**).

Table 2. Steady-state kinetic constants - K_m (μM), k_{cat} (s^{-1}) and k_{cat}/K_m (s^{-1} mM^{-1}) - of native VP and variants for VA and Mn^{2+} oxidation.

	VP[a]	W164S[b]	F198I	W244L	M247F[c]	M247L[c]	R257L[c]	M265L[d]

	K_m	4130 ± 320	-	-	-	4100 ± 400	6990 ± 630	13500 ± 600	3900 ± 300
VA	k_{cat}	9.5 ± 0.2	0	0	0	4.3 ± 0.2	5.0 ± 0.2	27.3 ± 0.5	11.4 ± 0.3
	k_{cat}/K_m	2.3 ± 0.1	0	0	0	1.1 ± 0.1	0.7 ± 0.0	2.0 ± 0.0	2.9 ± 0.2
	K_m	181 ± 10	110*	90 ± 7	120 ± 2	70 ± 5	82 ± 7	102 ± 9	136 ± 7
Mn^{2+}	k_{cat}	275 ± 4	207*	200 ± 3	165 ± 8	76 ± 1	150 ± 4	100 ± 2	215 ± 2
	k_{cat}/K_m	1520 ± 70	1900*	2220 ± 160	1340 ± 20	1090 ± 70	1830 ± 130	982 ± 76	1580 ± 103

[a,b,c,d], from refs. (40), (21), (41) and (42), respectively; *95% confidence limits below 10% of the mean values.

The analysis of the catalytic properties of the site-directed variants clearly shows that mutations W244L and F198I, at the *Phe's path*, turn the enzyme inactive against VA, in a similar fashion as when removing the surface tryptophan in the W164S variant. However, mutations in the *Met's path* (R257L and M265L) maintain the enzyme activity on VA, with similar catalytic efficiency values.

The M247L variant was also analyzed, and its residual activity suggests the possibility of direct electron transfer from Trp164 to Phe198 in the *Phe's path*, although Met247 occupies a neighbor position. Met247 was also substituted by a phenylalanine, the residue occupying this position in LiP (**Figure 2**) to investigate a possible relationship with the more efficient oxidation of VA by the latter enzyme, but no improvement was obtained.

Additional kinetic experiments were performed to oxidize Mn^{2+} directly at the propionate channel, in order to check whether these mutations affect other properties rather than the LRET region. Kinetic data, however, showed comparable values as the wild type (**Table 2**).

Thus, as predicted from the QM/MM e-pathway calculations, the experimental data confirmed that the *Phe's path* plays a major role in the LRET. Trp244, showing up in all computed paths top positions, has never been proposed as important for the electron transfer mechanism in VP, but has been recently proposed in LiP,[43] as discussed below. The importance of a phenylalanine residue homologous to Phe198 has been shown for high redox-potential substrate oxidation by a peroxidase variant.[44]

Overall, the results for VP clearly indicate that the LRET pathway should involve Trp164-Trp244-Phe198, finalizing in the proximal histidine which is directly bonded to the iron of the heme.

Analysis of LRET pathways in LiP. Similarity to VP, LiP is also able to oxidize different aromatic compounds through a surface tryptophan residue (LiPH8 Trp171), although it is more efficient oxidizing VA (K_m 190 ± 17 µM; k_{cat} 17.5 ± 0.5 s^{-1}; and k_{cat}/K_m 92.0 ± 6.0 $s^{-1}\cdot mM^{-1}$)[45] than VP (**Table 2**). This difference has been associated with a more acidic environment, better stabilizing the cation radical formed after VA oxidation.[10]

VA local diffusion with PELE was performed using the same parameters as employed for the simulation of VP. In agreement with the lower K_m observed in LiP, we find this time a better defined (sharper) minimum after the local sampling (**Figure 5, left**). VA, however, still presents multiple orientations, and those residues in contact with VA in the top representative poses are displayed in **Figure 5**. To unveil the LRET in LiP, the QM/MM e-pathway calculations were performed over five representative structures extracted from the PELE simulations (**Table 3)**.

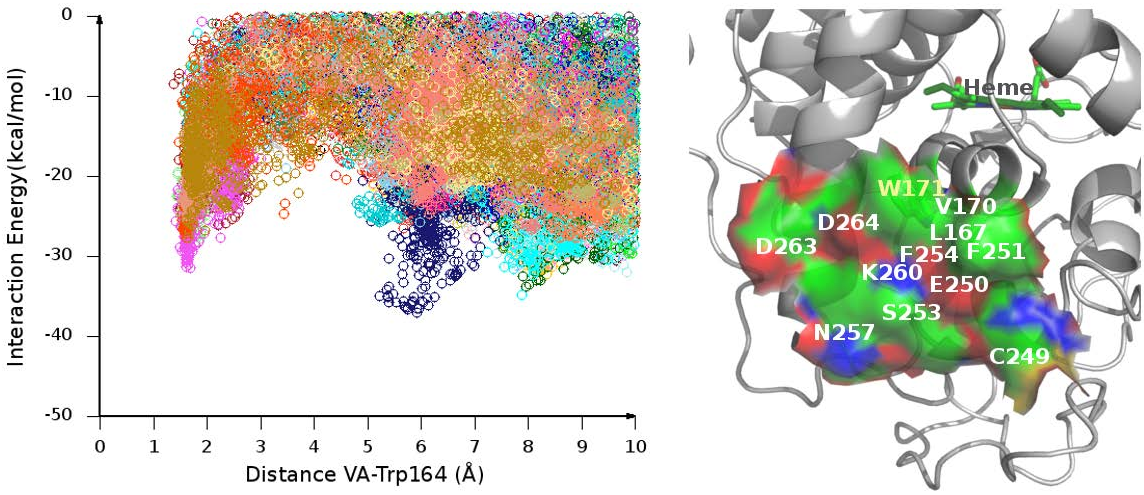

Figure 5. Substrate exploration in the environment of the catalytic Trp171 of LiP. *Left*: Interaction energy (kcal/mol) *vs* the lowest distance from any VA atom to Trp171 (HE1) in the local PELE diffusion simulations (120 CPUs x 48 h, each color represents a different processor). *Right*: Set of contact residues (within 4 Å) to VA in the best interaction energy structures (within 5 kcal/mol compared to the local minimum at ~2 Å).

Table 3. QM/MM e-pathway results (after seven iterations) from five different snapshots (sets 1-5) taken from the PELE diffusion of VA in LiP. Residues hosting the spin are listed (from left to right) in order of electron affinity.

	QM/MM iterations						
	1	*2*	*3*	*4*	*5*	*6*	*7*
set 1	F267 (bb)[a] I268 (bb)	W251	D264 (bb) F265 (bb) Q266 (bb)	F205 (bb)	W171	F193	F204 (bb)
set 2	Q266 (bb) F267 (bb)	F269(bb)	W251	F205 (bb)	D264 (bb)	A271 L272 (bb+sc)	F265
set 3	Q266 F267 (bb)	W251	F205	W171	D264 (bb) F265 (bb)	F254	M172
set 4	W251	I268 (bb) F267 (bb)	F205	W171 M172	D264 (bb) F265	F254	F193
set 5	W251	F267 (bb) I268 (bb)	F205	M172	D263 (bb) D264 F265 (bb)	W171	F254

[a] *bb* or *bb+sc* are specified when the spin density is located only at the residue's backbone or at both backbone and side-chain, respectively (in all the other cases, it is located only at the side chain).

Results show analogous paths to those obtained earlier for VP, where the main residues forming the *Phe's path* are conserved in LiP (**Figure 6**): Trp171 (VP Trp164), Trp251 (VP Trp244) and Phe205 (VP Phe198). However, the previously called *Met's path* does not present the methionines found in VP but two phenylalanines (Phe265 and Phe267, being Phe258 and Ala260 in VP, respectively) and one aspartic acid (Asp264, being Arg257 in VP), being, therefore, renamed as *Phe#2 path*.

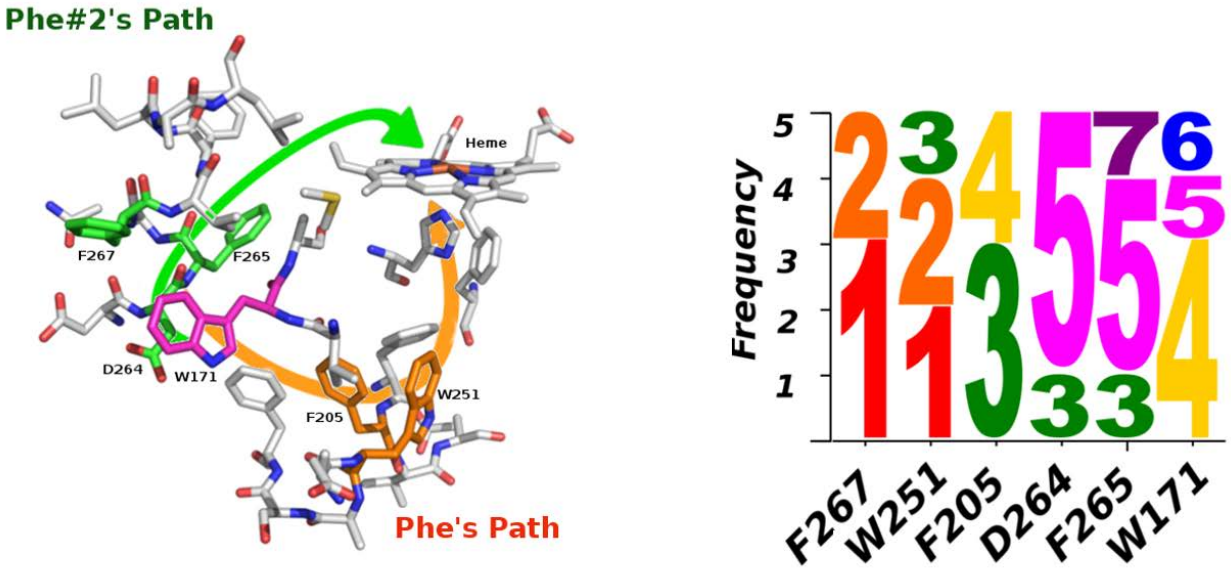

Figure 6. LiP electron transfer from Trp171 to heme. *Left*: Suggested LRET routes and neighbor residues. The catalytic residue (Trp171) is displayed in pink whereas the main residues found in the QM/MM e-pathway calculations are displayed in orange (*Phe's path*) and green (*Phe#2's path*). *Right*: Frequency of the positions found in the QM/MM e-pathways (data from Table 3) for the most common residues, found at least in four paths.

As previously found in VP, there is a second buried tryptophan residue, Trp251, which appears in all QM/MM e-pathway sets in a top ranked position together with the exposed Trp171, pointing again the predominance of the *Phe's path*. Notice that Phe267, also appearing as a top-ranked positions with Trp251, points rather a non-effective transfer to the heme (*cul-de-sac*). LiP Phe254 and Phe204 were not selected (as the homologous VP Met247 and Phe197, respectively) because they only appear in three and one of the predicted paths, respectively (**Table 3**).

The involvement of Trp251 in the LRET pathway of *P. chrysosporium* LiP was experimentally confirmed by site-directed mutagenesis to alanine. The resulting W251A variant showed three-fold lower catalytic efficiency oxidizing VA (66 ± 11 s^{-1} mM^{-1}) compared with native LiP8 (205 ± 4 s^{-1} mM^{-1}) due to k_{cat} decrease (from 16.2 ± 0.8 to 6.0 ± 0.3 s^{-1}), while the K_m was only slightly increased

(from 79 ± 18 to 91 ± 18 μM^{-1}). An even larger decrease of catalytic efficiency oxidizing a nonphenolic lignin model has been recently reported for the same LiP variant.[43] In addition, the strict requirement of Trp171 has been shown by site-directed mutagenesis using different lignin model compounds.[20,25] Thus, all these evidences indicate that, as observed in VP, the first *Phe's path* (here consisting of W171-Phe205-Trp251) is the main responsible for the LRET process.

Analysis of other VP and LiP sequences. Remarkably, the above buried tryptophan residue and the exposed catalytic tryptophan (W244/W251 and W164/W171 in *P. eryngii* VP/*P. chrysosporium* LiP, respectively) are conserved in all the 169 VP or LiP sequences available to date. Moreover, the third residue identified as part of the LRET pathway (F198/F205) also shows a high conservation degree, being in all cases phenylalanine or tyrosine residues (**Figure 7**).

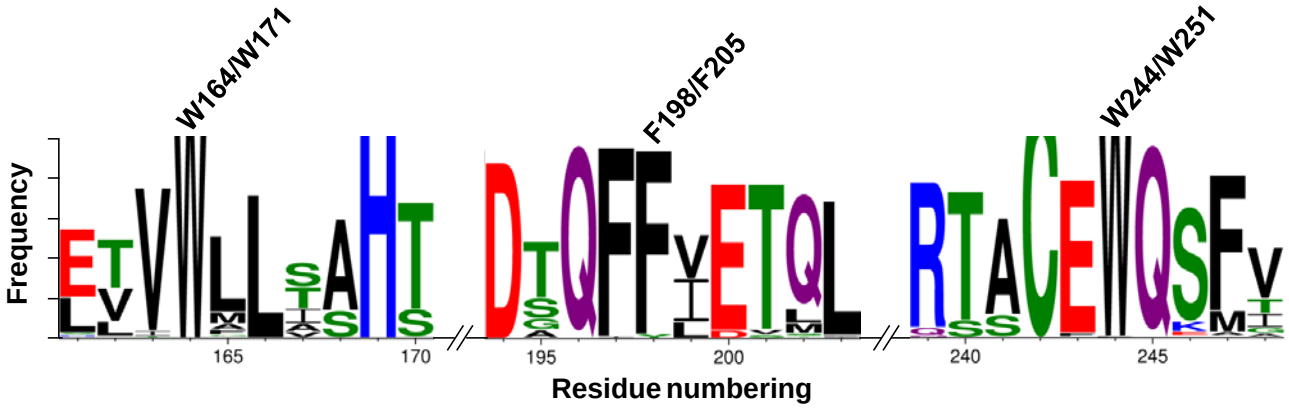

Figure 7. Sequence logo of three protein regions harboring residues involved in LRET from an exposed tryptophan to the heme cofactor in 169 peroxidases (92 LiPs and 77 VPs) available in GenBank database and genomes accessible through MycoCosm (www.jgi.doe.gov/fungi), prepared with Web Logo 3.5[46]. Residue numbering refers to *P. eryngii* VP (allelic variant VPL2). Numbering above the residues indicates the exposed tryptophan (W164/W171) and the two additional residues (F198/F205 and W244/W251) identified by QM/MM e-pathway[27,28] in *P. eryngii* VP/*P. chrysosporium* LiP.

Identification of such LRET route was possible by the use of computational tools, and contrasts with the former hypothesis suggesting direct transfer from the catalytic tryptophan (Trp164/Trp171 of VP/LiP) to the heme (methyl-C group) through the side-chain of the contiguous residue

(Leu165/Met172).[21] Moreover, conservation of the same route among the different ligninolytic peroxidases, as suggested by the screening of basidiomycete genomes, strongly supports its relevance in lignin degradation by fungal LiPs and VPs.

CONCLUSIONS

Experimental and computational efforts were made to study the VP oxidation of VA (as a simple lignin model compound) through an intramolecular LRET mechanism. In this case, computational methodologies avoid making extensive trial-error mutagenic experiments in order to establish the residues in the path (and the side-chain or backbone contribution). Instead, the data obtained from the QM/MM e-pathway technique assists in designing an experiment to identify the pathway undertaken by the electron. From the computational analysis we first identified two possible routes in VP beginning both with Trp164, which has been characterized in previous studies as the VP residue oxidizing VA.[21] The calculations, moreover, indicate the importance of a second buried tryptophan residue, Trp244. From these results, some mutants were designed involving residues from both paths in order to identify the most favorable route. Experimental evidence showed a lack of reactivity when residues Phe198 and Trp244 were mutated, while around 50% activity remained for the M256L mutant and no significant changes were observed for R257L and M265L (the two latter in the *Met's path*). Therefore, we can conclude the transfer occurs through the *Phe's path,* including Trp164, Trp244 and Phe198. Interestingly, equivalent results are found for LiP, where two routes (from Trp171) were also obtained by the QM/MM e-pathway calculations. In LiP, we find again the importance of a second tryptophan residue, Trp251, in agreement with directed mutagenesis experiments. These results, together with the conservation of the above residues after sequence screening in genomes, indicate the involvement of an analogous electron transfer pathway, the *Phe's path*, in the long-range oxidation mechanism of VP and LiP from different basidiomycetes. Such mechanism was a crucial evolutionary acquisition in ligninolytic peroxidases since it enabled electron

abstraction from lignin (whose bulky nature prevents direct interaction with the activated cofactor) at the protein surface, as it has been recently demonstrated for *P. eryngii* VP and *P. chrysosporium* LiP.[19,47]

AUTHOR INFORMATION

Corresponding authors

*E-mail guallarv@gmail.com; Phone +34 934137727 (V.G.)

*E-mail ATMartinez@cib.csic.es; Phone +34 918373112 (A.T.M.)

ORCID

S. Acebes: 0000-0001-8854-654X

F.J. Ruiz-Dueñas: 0000-0002-9837-5665

M. Toubes: 0000-0001-7884-7285

V. Sáez-Jiménez: 0000-0001-7043-5622

M. Pérez-Boada: 0000-0002-3288-0853

M.F. Lucas: 0000-0001-8672-9940

A.T. Martínez: 0000-0002-1584-2863

V. Guallar: 0000-0002-4580-111

Present addresses

[1]School of Engineering and Material Science. Yale University, 10 Hillhouse Ave, New Haven, CT 06511, EE.UU (sandra.acebes@yale.edu) (S.A.)

[2]School of Science and the Environment, Manchester Metropolitan University, Manchester, M1 5GD, UK (m.rodrigo@mmu.ac.uk) (M.T.)

[3]Department of Biology and Biological Engineering, Chalmers University of Technology, 41296 Gothenburg, Sweden (saez@chalmers.se) (V.S.-J.)

Notes

The authors declare no competing interest.

ACKNOWLEDGEMENT

This work was supported by the INDOX (KBBE-2013-7-613549) EU project, and by the projects EnzOx2 (H2020-BBI-PPP-2015-2-720297) of the Joint Undertaking of European BioBased Industries (www.bbi-europe.eu), and BIO2014-56388-R (NOESIS) and CTQ2016-79138-R of the Spanish Ministry of Economy and Competitiveness (MINECO). F.J.R.-D. acknowledges a MINECO Ramón & Cajal contract.

ABBREVIATIONS

DTT, dithiothreitol; k_{cat}, catalytic constant; K_m, Michaelis constant; LiP, lignin peroxidase; LRET, long-range electron transfer; MnP, manganese peroxidase; PELE, Protein Energy Landscape Exploration (software); QM/MM, quantum mechanics and molecular mechanics; VA, veratryl alcohol; VP, versatile peroxidase

REFERENCES

1. Zámocký, M.; Hofbauer, S.; Schaffner, I.; Gasselhuber, B.; Nicolussi, A.; Soudi, M.; Pirker, K. F.; Furtmüller, P. G.; Obinger, C. Independent evolution of four heme peroxidase superfamilies. *Arch. Biochem. Biophys.* **2015**, *574*, 108-119.
2. Ruiz-Dueñas, F. J.; Martínez, A. T. Microbial degradation of lignin: How a bulky recalcitrant polymer is efficiently recycled in nature and how we can take advantage of this. *Microbial Biotechnol*. **2009**, *2*, 164-177.
3. Hammel, K. E.; Cullen, D. Role of fungal peroxidases in biological ligninolysis. *Curr. Opin. Plant Biol.* **2008**, *11*, 349-355.
4. Martínez, A. T.; Ruiz-Dueñas, F. J.; Martínez, M. J.; del Río, J. C.; Gutiérrez, A. Enzymatic delignification of plant cell wall: from nature to mill. Curr. Opin. Biotechnol. **2009**, *20*, 348-357.
5. Ragauskas, A. J.; Williams, C. K.; Davison, B. H.; Britovsek, G.; Cairney, J.; Eckert, C. A.; Frederick, W. J.; Hallett, J. P.; Leak, D. J.; Liotta, C. L. et al. T. The path forward for biofuels and biomaterials. *Science*. **2006**, *311*, 484-489.
6. Ragauskas, A. J.; Beckham, G. T.; Biddy, M. J.; Chandra, R.; Chen, F.; Davis, M. F.; Davison, B. H.; Dixon, R. A.; Gilna, P.; Keller, M. et al. Lignin valorization: improving lignin processing in the biorefinery. *Science*. **2014**, *344*, 1246843.
7. Gupta, V. K.; Tuohy, K. *Microbial enzymes in bioconversions of biomass*; Springer, 2016.
8. Martínez, A. T.; Camarero, S.; Ruiz-Dueñas, F. J.; Martínez, M. J. Biological lignin degradation. In Lignin valorization: Emerging Approaches (Beckham, G. T.; ed) pp. 1-27, Royal Society of Chemistry, 2017.
9. Pollegioni, L.; Tonin, F.; Rosini, E. Lignin-degrading enzymes. *FEBS J.* **2015**, *282*, 1190-1213

10. Martínez, A. T. Molecular biology and structure-function of lignin-degrading heme peroxidases. *Enzyme Microb. Technol.* **2002**, *30*, 425-444.
11. Poulos, T. L. Heme enzyme structure and function. *Chem. Rev.* **2014**, *114*, 3919-3962
12. Gold, M. H.; Youngs, H. L.; Gelpke, M. D. Manganese peroxidase. *Met. Ions Biol. Syst.* **2000**, *37*, 559-586.
13. Ruiz-Dueñas, F. J.; Morales, M.; García, E.; Miki, Y.; Martínez, M. J.; Martínez, A. T. Substrate oxidation sites in versatile peroxidase and other basidiomycete peroxidases. *J. Exp. Bot.* **2009**, *60*, 441-452.
14. Floudas, D.; Binder, M.; Riley, R.; Barry, K.; Blanchette, R. A.; Henrissat, B.; Martínez, A. Y.; Otillar, R.; Spatafora, J. W.; Yadav, J. S. et al. The Paleozoic origin of enzymatic lignin decomposition reconstructed from 31 fungal genomes. *Science*. **2012**, *336*, 1715-1719.
15. Fernández-Fueyo, E.; Acebes, S.; Ruiz-Dueñas, F. J.; Martínez, M. J.; Romero, A.; Medrano, F. J.; Guallar, V.; Martínez, A. T.Structural implications of the C-terminal tail in the catalytic and stability properties of manganese peroxidases from ligninolytic fungi. *Acta Crystallogr., Sect. D: Biol. Crystallogr.* **2014**, *70*, 3253-3265.
16. Morales, M.; Mate, M. J.; Romero, A.; Martínez, M. J.; Martínez, Á. T.; Ruiz-Dueñas, F. J. Two oxidation sites for low redox potential substrates: A directed mutagenesis, kinetic, and crystallographic study on *Pleurotus eryngii* versatile peroxidase. *J. Biol. Chem.* **2012**, *287*, 41053-41067.
17. Pogni, R.; Baratto, M. C.; Teutloff, C.; Giansanti, S.; Ruiz-Dueñas, F. J.; Choinowski, T.; Piontek, K.; Martínez, A. T.; Lendzian, F.; Basosi, R. A tryptophan neutral radical in the oxidized state of versatile peroxidase from *Pleurotus eryngii:* A combined multi-frequency EPR and DFT study. *J. Biol. Chem.* **2006**, *281*, 9517-9526.

18. Smith, A. T.; Doyle, W. A.; Dorlet, P.; Ivancich, A. Spectroscopic evidence for an engineered, catalytically active Trp radical that creates the unique reactivity of lignin peroxidase. *Proc. Natl. Acad. Sci. USA.* **2009**, *106*, 16084-16089.

19. Sáez-Jiménez, V.; Rencoret, J.; Rodríguez-Carvajal, M. A.; Gutiérrez, A.; Ruiz-Dueñas, F. J.; Martínez, A. T. Role of surface tryptophan for peroxidase oxidation of nonphenolic lignin. *Biotechnol. Biofuels.* **2016**, *9*,198.

20. Dunford, H. B. *Peroxidases and catalases: Biochemistry, biophysics, biotechnology and physiology*; John Wiley & Sons: New York, 2010.

21. Pérez-Boada, M.; Ruiz-Dueñas, F. J.; Pogni, R.; Basosi, R.; Choinowski, T.; Martínez, M. J.; Piontek, K.; Martínez, A. T. Versatile peroxidase oxidation of high redox potential aromatic compounds: Site-directed mutagenesis, spectroscopic and crystallographic investigations of three long-range electron transfer pathways. *J. Mol. Biol.* **2005**, *354*, 385-402.

22. Doyle, W. A.; Blodig, W.; Veitch, N. C.; Piontek, K.; Smith, A. T. Two substrate interaction sites in lignin peroxidase revealed by site-directed mutagenesis. *Biochemistry*. **1998**, *37*, 15097-15105.

23. Choinowski, T.; Blodig, W.; Winterhalter, K. H.; Piontek, K. . The crystal structure of lignin peroxidase at 1.70 Å resolution reveals a hydroxy group on the Cβ of tryptophan 171: A novel radical site formed during the redox cycle. *J. Mol. Biol.* **1999**, *286*, 809-827.

24. Blodig, W.; Smith, A. T.; Doyle, W. A.; Piontek, K. Crystal structures of pristine and oxidatively processed lignin peroxidase expressed in *Escherichia coli* and of the W171F variant that eliminates the redox active tryptophan 171. Implications for the reaction mechanism. *J. Mol. Biol.* **2001**, *305*, 851-861.

25. Mester, T.; Ambert-Balay, K.; Ciofi-Baffoni, S.; Banci, L.; Jones, A. D.; Tien, M. Oxidation of a tetrameric nonphenolic lignin model compound by lignin peroxidase. *J. Biol. Chem.* **2001**, *276*, 22985-22990.

26. Kurnikov, I. *HARLEM molecular modeling package.* Department of Chemistry, University of Pittsburgh: Pittsburgh, PA, 2000.

27. Guallar, V.; Wallrapp, F. Mapping protein electron transfer pathways with QM/MM methods. *J. R. Soc. Interface.* **2008**, *5*, 233-239.

28. Guallar, V.; Heme electron transfer in peroxidases: The propionate e-pathway. *J. Phys. Chem. B.* **2008**, *112*, 13460-13464.

29. Linde, D.; Pogni, R.; Cañellas, M.; Lucas, F.; Guallar, V.; Baratto, M. C.; Sinicropi, A.; Sáez-Jiménez, V.; Coscolín, C.; Romero, A. et al. Catalytic surface radical in dye-decolorizing peroxidase: A computational, spectroscopic and directed mutagenesis study. Biochem.J. 466,253-262, 2015.Catalytic surface radical in dye-decolorizing peroxidase: A computational, spectroscopic and directed mutagenesis study. *Biochem. J.* **2015**, *466*, 253-262.

30. Sastry, G. M.; Adzhigirey, M.; Day, T.; Annabhimoju, R.; Sherman, W. Protein and ligand preparation: Parameters, protocols, and influence on virtual screening enrichments. *J. Comput.-aided Mol. Design.* **2013**, *27*, 221-234.

31. Li, H.; Robertson, A. D.; Jensen, J. H., Very fast empirical prediction and rationalization of protein pKa values. *Protein-Struct. Funct. Bioinf.* **2005**, *61*,704-721.

32. Murphy, R. B.; Philipp, D. M.; Friesner, R. A. A mixed quantum mechanics/molecular mechanics (QM/MM) method for large-scale modeling of chemistry in protein environments. *J. Comput. Chem.* **2000**, *21*, 1442-1457.

33. Borrelli, K. W.; Vitalis, A.; Alcantara, R.; Guallar, V. PELE: protein energy landscape exploration. A novel Monte Carlo based technique. *J. Chem. Theory Comput.* **2005**, *1*, 1304-1311.

34. Acebes, S.; Fernandez-Fueyo, E.; Monza, E.; Lucas, M. F.; Almendral, D.; Ruiz-Dueñas, F. J.; Lund, H.; Martínez, A. T.; Guallar, V. Rational enzyme engineering through biophysical and biochemical modeling. *ACS Catal.* **2016**, *6*, 1624-1629.

35. Bowers, K. J.; Chow, E.; Xu, H.; Dror, R. O.; Eastwood, M. P.; Gregersen, B. A.; Klepeis, J. L.; Kolossvary, I.; Moraes, M. A.; Sacerdoti, F. D. et al. Scalable algorithms for molecular dynamics simulations on commodity clusters. *Proc. ACM/IEEE Conference on Supercomputing (SC06), Tampa, 11-17 November,* p. 84.

36. Cohen, A.J.; Mori-Sánchez, P.; Yang, W. Insights into current limitations of density functional theory. *Science*. **2008**, *321*,792-794.

37. Pérez-Boada, M.; Doyle, W. A.; Ruiz-Dueñas, F. J.; Martínez, M. J.; Martínez, A. T.; Smith, A. T. Expression of *Pleurotus eryngii* versatile peroxidase in *Escherichia coli* and optimisation of *in vitro* folding. *Enzyme Microb. Technol.* **2002**, *30*, 518-524.

38. Sambrook, J.; Fritsch, E. F.; Maniatis, T. *Molecular cloning. Vol. 2*; Cold Spring Harbor Laboratory Press: New York, 1989.

39. Recabarren, R.; Fuenzalida-Valdivia, I.; Alzate-Morales, J. Studying the binding mechanisms of veratryl alcohol to *P. chrysosporium* lignin peroxidase: Insights from theoretical approaches. *Theor. Chem. Acc.* **2016**, *135*, 1-12.

40. Ruiz-Dueñas, F. J.; Pogni, R.; Morales, M.; Giansanti, S.; Mate, M. J.; Romero, A.; Martínez, M. J.; Basosi, R.; Martínez, A. T. Protein radicals in fungal versatile peroxidase: Catalytic tryptophan radical in both Compound I and Compound II and studies on W164Y, W164H and W164S variants. *J. Biol. Chem.* **2009**, *284*, 7986-7994.

41. Ruiz-Dueñas, F. J.; Morales, M.; Mate, M. J.; Romero, A.; Martínez, M. J.; Smith, A. T.; Martínez, A. T. Site-directed mutagenesis of the catalytic tryptophan environment in *Pleurotus eryngii* versatile peroxidase. *Biochemistry*. **2008**, *47*, 1685-1695.

42. Sáez-Jiménez, V.; Acebes, S.; Guallar, V.; Martínez, A. T.; Ruiz-Dueñas, F. J. Improving the oxidative stability of a high redox potential fungal peroxidase by rational design. *PLoS One.* **2015**, *10*(4):e0124750.

43. Pham, L. T. M.; Kim, S. J.; Kim, Y. H. Improvement of catalytic performance of lignin peroxidase for the enhanced degradation of lignocellulose biomass based on the imbedded electron-relay in long-range electron transfer route. *Biotechnol. Biofuels.* **2016**, *9*, 247.

44. Fernández-Fueyo, E.; Ruiz-Dueñas, F. J.; Miki, Y.; Martínez, M. J.; Hammel, K. E.; Martínez, A. T. Lignin-degrading peroxidases from genome of selective ligninolytic fungus *Ceriporiopsis subvermispora*. *J. Biol. Chem.* **2012**, *287*, 16903-16916.

45. Fernández-Fueyo, E.; Ruiz-Dueñas, F. J.; Martínez, A.T. Engineering a fungal peroxidase that degrades lignin at very acidic pH. *Biotechnol. Biofuels.* **2014**, *7*, 114.

46. Crooks, G. E.; Hon, G.; Chandonia, J. M.; Brenner, S. E. WebLogo: A sequence logo generator. *Genome Res.* **2004**, *14*, 1188-1190.

47. Sáez-Jiménez, V.; Baratto, M. C.; Pogni, R.; Rencoret, J.; Gutiérrez, A.; Santos, J. I.; Martínez, A. T.; Ruiz-Dueñas, F. J. Demonstration of lignin-to-peroxidase direct electron transfer: A transient-state kinetics, directed mutagenesis, EPR and NMR study. *J. Biol. Chem.* **2015**, *290*, 23201-23213.

TOC Graphics: